Applied Physics A (2023) 129:160
https://doi.org/10.1007/s00339-023-06414-6

Applied Physics A
Materials Science & Processing

S.I. : 50TH ANNIVERSARY OF APPLIED PHYSICS

Continuous wave laser grooving of cementitious materials

Marco Rupp[1,2] · Shuichiro Hayashi[1,2,3] · Claire Dashe[1,2] · Shashank Gupta[2,4] · Reza Moini[2,4] · Craig B. Arnold[1,2]

Received: 27 November 2022 / Accepted: 11 January 2023 / Published online: 1 February 2023

Abstract
Fracture examination of brittle and quasi-brittle materials typically requires the creation of a sharp notch that involves removal of solid materials to nucleate a crack at a well-defined location. Here, we investigate the use of a 400 W continuous wave laser to create well-defined grooves in hardened cement-based materials. The influence of scanning speeds of a laser on the processing of cement-based materials was investigated using scanning electron microscopy (SEM) and confocal microscopy. The results show that for constant laser power below a certain scanning speed, redeposition of the material in the form of bridges across the groove decreases the effectiveness of the cut leading to an optimal combination of speed and laser power for sharp groove formation. Grooving cementitious material by laser processing enables significantly smaller grooves than those created using conventional methods, such as circular saws, and allows more precise control over location and cutting depth.

Keywords Laser processing · Cement paste · Sample preparation · Groove formation

1 Introduction

Cementitious materials are the backbone of civil infrastructure and building material acting as the binder in concrete as a particle-reinforced composite [1]. Due to their function, understanding the mechanical properties of cementitious materials plays a vital role in optimizing the composition and ultimate properties of the infrastructure components [2]. Typical experimental fracture characterization methods used for brittle and quasi-brittle cementitious materials, such as compact tension test, single-edge notched beam test, and wedge split test, require the creation of a notch in the material with well-defined sharpness [3–6]. However, sensitivity to notch shape, size, and geometry can be particularly challenging in brittle materials [7–10]. Traditional notch creation in hard materials is done using circular saws equipped with thick (several mm) [11] diamond blades [12]. Diamond blades are quite effective and come at a moderate cost; however, they are limited in their ability to create narrow kerfs and can create dust and other health hazards that require proper management [13]. Additionally, and perhaps more importantly, the base of these grooves tends to be flat or 'U' shaped as compared to the desired 'V' shape for the determination of accurate fracture study [14, 15]. Although the capital cost for a laser is more expensive, they increase flexibility of the processing. For instance, laser processing has traditionally been applied for cutting concrete using high powers [16–19], but little work has been done to use laser for creating notches and intentional defects [20].

In this work, we explore the use of continuous wave (CW) laser processing to create 'V' shaped grooves in hardened cement paste at fixed laser power but different scanning speeds. We find that the laser process can produce the desired sharp notches with steep side walls under the right processing conditions. Outside the optimal conditions, recast and restructuring of the groove sidewalls create bridges within the notch (or ahead of the notch tip) that can potentially be detrimental to the microstructure or lead to inaccurate fracture properties. The effects of laser processing on the microstructure are investigated using scanning electron microscopy (SEM) and confocal microscopy.

✉ Craig B. Arnold
cbarnold@princeton.edu

[1] Department of Mechanical and Aerospace Engineering, Princeton University, Olden St., Princeton, NJ 08544, USA

[2] Princeton Institute for the Science and Technology of Materials, Princeton University, Prospect Ave., Princeton 08540, USA

[3] School of Integrated Design Engineering, Keio University, 3-14-1, Hiyoshi, Kohoku-ku, Yokohama, Kanagawa 223-8522, Japan

[4] Department of Civil and Environmental Engineering, Princeton University, Olden St., Princeton, NJ 08544, USA

2 Materials and methods

2.1 Materials and sample preparation

The cement paste samples were fabricated using Ordinary Portland Cement (OPC) and a water-to-cement ratio of 0.275 based on previous studies [21]. A type I/II ordinary portland cement (OPC) (ASTM C150-07) was used in this study and its chemical composition and physical properties can be found in Table 1. The Blaine fineness of the OPC used in this study was 412 m^2/kg, and its fineness 325 Sieve (passing) was 91.4%. A high range water reducing admixture (HRWR, MasterGlenium 7700) and viscosity modifying admixture (VMA, MasterMatrix 362) were used in this study (ASTM C494/C494M-08). The mixture consisted of 250 g of cement, 1.47 g of HRWR, 2.38 g of VMA, and 65.50 g of water. After weighing the materials, water was placed in the mixing bowl then VMA and HRWR were added and dispersed using a spatula. Cement was then added to the liquid solution and mixed for 90 s at 400 revolutions per minute (rpm) in a twister evolution Venturi vacuum mixer at 70% vacuum level. The vacuum was stopped for 15 s to scrape down in the mixing bowl any paste that may have collected to the side of the bowl. The cement paste was then mixed for additional 90 s at 400 rpm at 100% vacuum level [21]. The fresh cement paste was prepared in a rectangular 3D-printed PLA mold for casting and curing. The dimensions of the cement paste samples are $40 \times 40 \times 15$ mm^3. The samples were kept at a $93 \pm 2\%$ relative humidity using saturated solutions of potassium nitrate were kept for 3 days [21]. The chemical composition of the samples is described in Table 1. After the curing process and hardening of the cement paste was completed, the samples were moved to the laser apparatus for grooving.

Table 1 Oxides and Bogue composition and physical property of the cement

Cement oxides	Type I/II cement (OPC)
	Percentage by mass (%)
Silicon dioxide (SiO_2)	19.60
Aluminum oxide (Al_2O_3)	4.40
Ferric oxide (Fe_2O_3)	2.90
Calcium oxide (CaO)	60.70
Magnesium oxide (MgO)	3.70
Sulfur trioxide (SO_3)	4.50
Equivalent alkali (Na_2O_{eq})	0.75
Loss on ignition (LOI)	2.30
Bogue phase composition	Percentage by mass (%)
Tricalcium silicate (C_3S)	52.00
Dicalcium silicate (C_2S)	17.00
Tricalcium aluminate (C_3A)	7.00
Tetracalcium aluminoferrite (C_4AF)	9.00
Specific gravity	3.15

2.2 Experimental method

A schematic of the experimental setup can be seen in Fig. 1. A hardened cement paste specimen was placed underneath the laser inside a testing chamber. The laser was programmed to move the beam over the sample with the pre-set geometric conditions of a simple line and a power of 400 W. A gas outlet with a diffuser was mounted inside the testing chamber to ensure that no particles were deposited in the path of the laser before or after the passing.

In this setup, a 1070 nm wavelength laser operating in CW mode was used as the laser source. The laser (YLR-400-AC) has a maximum power of 400 W with a beam diameter of 100 µm. The laser beam passes through the 3D scanning system after being narrowed by a focusing telescope. The computer-controlled 3D scanning system consists of a beam expander, a 2D scanner, and an F–θ lens with a scan field of 178 by 178 mm^2. The laser irradiation was set to the maximum power, while the rastering speed was varied between 15 and 50 mm/s. The groove was fabricated by a single pass and the laser path was programmed to be longer

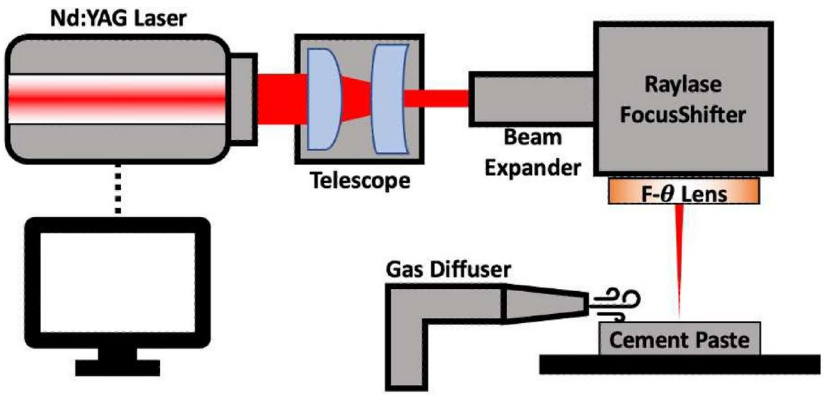

Fig. 1 Schematic of the experimental setup highlighting the hardened cement paste block underneath the laser

than the sample to avoid any potential edge effects in the sample. At these speeds, it takes only seconds to create a groove across the 40 mm-wide × 15 mm-thick hardened cement paste sample.

2.3 Evaluation method

After irradiating the cement paste samples, the size of the resulting kerf on the sample surface was measured using the software available on the confocal microscope. Each cement paste sample had multiple parallel grooves. To determine the depth of the laser grooves, the samples were broken in half and polished with sandpaper, and the resulting cross-sections were observed with microscopy. The surface topology was analyzed using a confocal microscope (VK-X3050 Confocal, Keyence, Japan) and a scanning electron microscope (Quanta 200 FED, FEI, USA).

3 Results and discussion

Figure 2 provides an example of a top view of one of the cement samples highlighting the laser grooves. The top groove was created with a scanning speed of 30 mm/s and the bottom groove was created using a rastering speed of 25 mm/s. The grooves differentiate themselves from the bulk of the material by color. The bulk has heterogeneous grayish surface color, whereas the grooves are darker, shinier, and smoother. In this paper, the kerf size of a groove is defined as the distance between the color changes.

Figure 3 shows a top view of a laser groove generated by a 50 mm/s and 15 mm/s laser rastering speed. The figure shows the unirradiated surfaces above and below the groove. In comparison to the confocal image, the SEM images reveal more about the microstructure. The material shows clear signs of decomposed or melted regions on the sidewalls of the groove. The faster scanning speed of 50 mm/s (Fig. 3a) shows a deep and sharp groove with rough side walls, whereas the slower scanning speed of 15 mm/s (Fig. 3b) shows small cracks surrounding the groove. Notably, the slower scanning speed shows 'bridges' across the groove (i.e., notch bridging) and smaller air pockets which is hypothesized to have been formed from resolidified molten material. The cracks appeared in both the resolidified material and the surrounding cement paste (along and perpendicular to the groove) that was not directly lasered.

Comparing the two images, it is apparent that the slower scanning speed led to more removal of the material and created a larger kerf corresponding to the relative larger energy per unit area as compared to the faster scanning speed. This leads to deeper and wider decomposed or melt pools during the laser process [22, 23]. In addition, the higher temperatures extending into the surrounding cement paste leads to

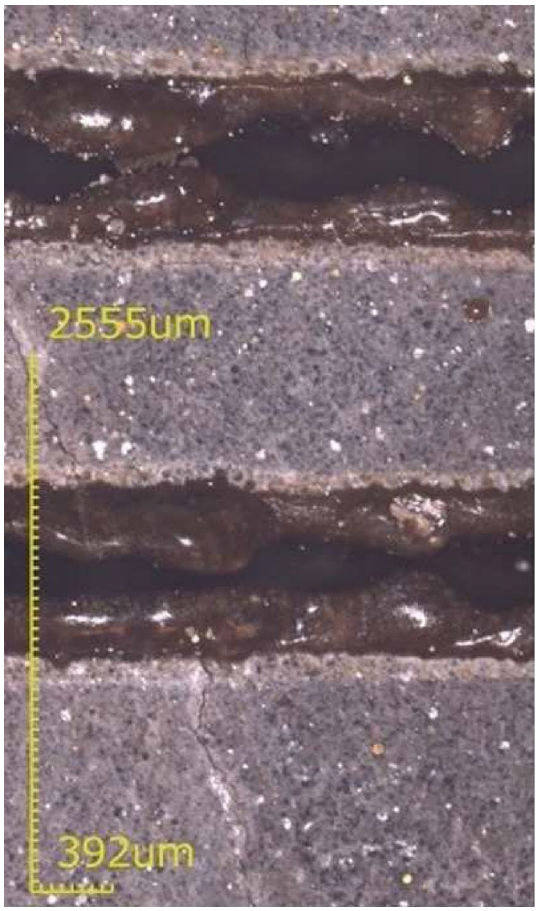

Fig. 2 Schematic of the experimental setup highlighting the hardened cement paste block underneath the laser

additional modifications, such as dehydration [24], decomposition [25], and melting [26], as well as crack formation due to the stress generated upon cooling. However, the main difference between the slow and fast scanning speed images is the appearance of glassy bridges across the groove. This deposition is unwanted, since it creates a hard glass structure across with bridges and air pockets along the groove in addition to adjacent cracking, and, therefore, would be expected to affect any subsequent mechanical and fracture testing.

Figure 4 shows the cross-section of a hardened cement paste sample with four grooves. The scanning speed for these grooves was 50 mm/s, 40 mm/s, 30 mm/s, and 25 mm/s, respectively, from top to bottom. Examining the grooves allows us to define two different groove depths: the impacted depth and the clear depth. The impacted depth is the maximum depth the laser reached during the grooving. This is indicated by the maximum depth at which the material exhibits a color change in the optical images. Conversely, the clear depth is the maximum depth the laser achieved before any bridging occurs. In Fig. 4, the impacted depth gets deeper as the laser speed decreases. However, as

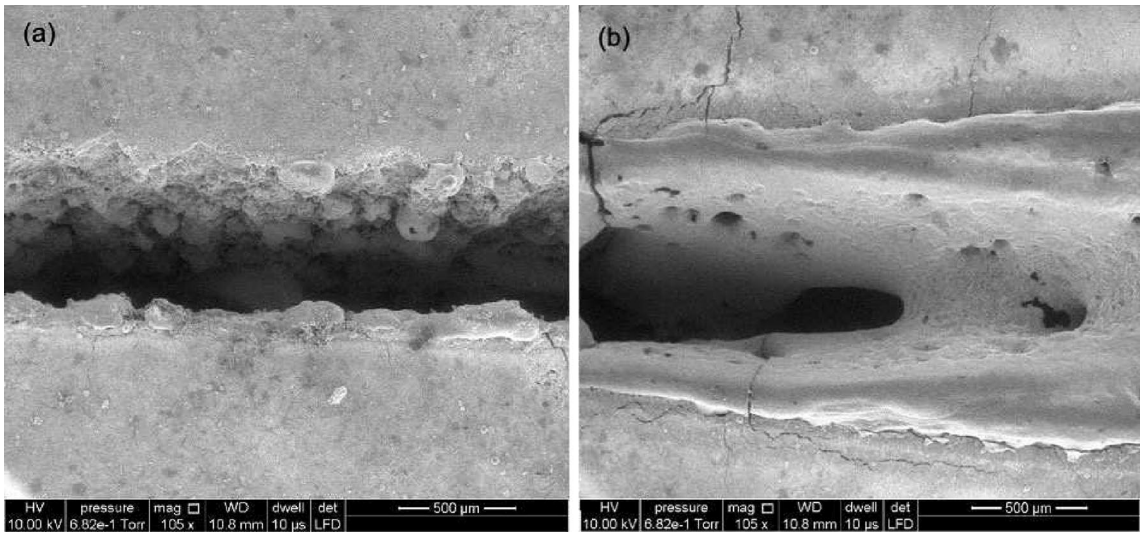

Fig. 3 Top view of a hardened cement paste sample with a laser groove with scanning speed of **a** 50 mm/s and **b** 15 mm/s. The image was acquired via SEM and shows small cracks surrounding the kerf, where the laser groove is

Fig. 4 Cross-sectional view of a hardened cement paste sample. Optical comparison of hardened cement paste containing grooves with 50 mm/s, 40 mm/s, 30 mm/s, and 25 mm/s (top to bottom). **a** Confocal microscope image of various grooves using laser and optical information. **b** Confocal microscope image with height information, confirming the depth of the grooves. There is no quantifiable depth associated with the green color

the depth increases, we notice that the grooves begin to show increasing sidewall roughness leading to bridging.

The groove depths from Fig. 4 can be quantified as a function of scanning speed, and the results are shown in Fig. 5. The impacted depth decreases with respect to the increasing scanning speed. This general trend is expected from the decreasing energy per unit area as the speed increases. In comparison to the impacted depth, the clear depth follows a more complicated trend. For high scan speeds, the two depths are approximately equal indicating that the laser process is completely clearing material out from the groove as it passes. However, below 35 mm/s, the two depths diverge with the clear depth decreasing as the scanning speed is decreased further. This result is expected for the same reason. As the scanning speed decreases, the groove depth (and width) increases; thus, there is a greater volume of material

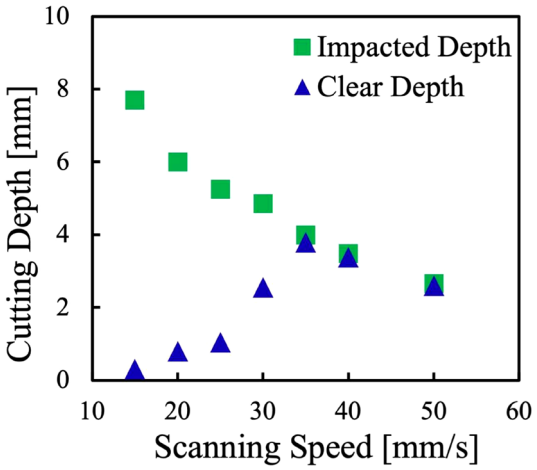

Fig. 5 Grooving depths of different scanning speeds with a constant power of 400 W. The gathered data show an overall trend of decreasing grooving depth for increasing scanning speed for the impacted depth. For fast scanning speeds, the impacted depth is very close to the clear depth, but for slow scanning speeds, the clear depth is lower than the impacted depth

to be removed. However, as the impact depth increases, it becomes more energetically difficult to cleanly remove all the material due to increasing depth of recast material and sidewall roughness. This effect is commonly observed in laser ablation of metals and semiconductor materials [27, 28]. For future work, different laser powers can be explored to find a quantitative relationship between scanning speed, laser power, clear depth, and impacted depth. Finally, Fig. 6 shows that similar to the impacted depth, a decrease in laser speed leads to an increase in kerf. The kerf versus scanning speed follows a linear trend and the downward slope is expected to continue until the laser speed is too fast to melt, decompose, or remove any material. The kerf versus scanning speed further supports the analysis for impact depth above.

4 Conclusion

Engineering defects in engineered materials or accurate notch formation for examination of fracture response of brittle materials are critical for obtaining accurate and meaningful data. Laser grooving has the potential to enable this in cementitious materials by providing control over the spatial and energy domains. Through control over laser processing parameters, it is possible to control the notch width and depth all while maintaining a clear 'V' shaped groove in the material. For fixed laser power, as the scanning speed decreases, the depth and the width increase until a critical speed is reached. Below that speed, the laser process is unable to cleanly remove all the material and creates resolidified bridges across the groove that structurally support the notch. As a result, a new measure is defined to distinguish the clear depth of the groove from the impacted depth (i.e., the maximum depth affected by the laser process). We would expect that the optimal processing conditions for subsequent material notching would be those for which the clear depth and the impact depth are the same resulting in a sharp 'V' shaped groove in the material. Otherwise, defects within the notch (or ahead of the notch tip) would alter the length of the fracture process zone and the resulting fracture toughness properties. In our experiments with a 400 W laser, the

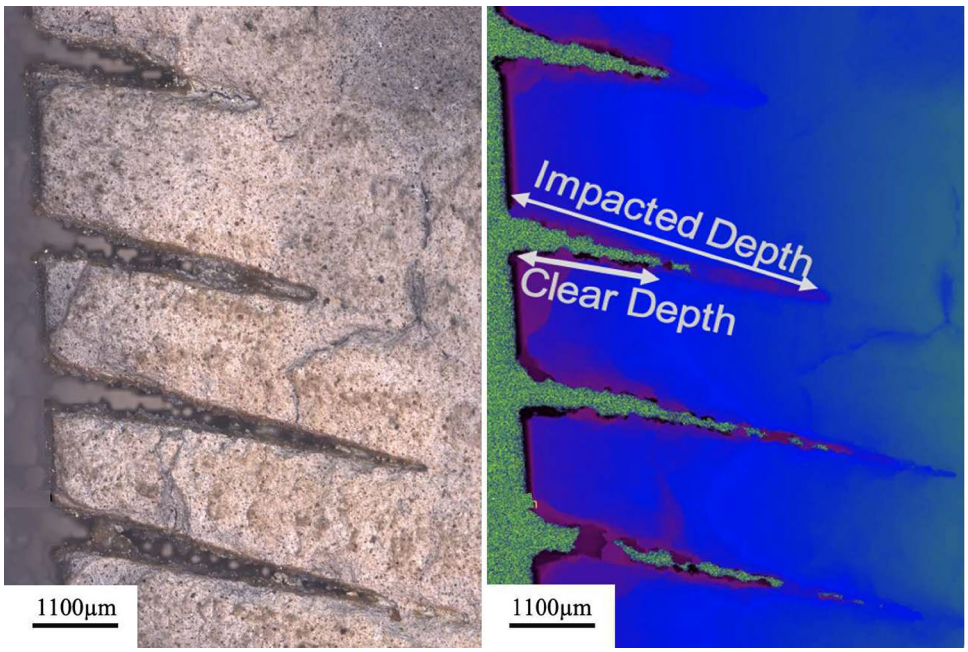

Fig. 6 Kerf width of different scanning speeds with constant laser power of 400 W. The data show a linear trend, where the kerf decreases with increasing laser speed. Similarly to the trend observed for the impacted depth in Fig. 5, the kerf decreases with increasing laser speed. This can be explained by an increase in deposited energy per unit area for slower scan speeds

critical scanning speed is 35 mm/s which results in a 4 mm deep × 0.75 mm wide clear groove across the sample. Inevitably, it is expected that higher power lasers would enable much faster speeds leading to a precise and commercially viable laser-based approach for creating grooves and engineered defects in concrete and other brittle or quasi-brittle infrastructure material. Future studies will provide a meaningful guide to understanding how the process can be scaled up and be applied to different materials and industries.

Author Contributions All authors contributed to the study conception and design. MR performed the laser and characterization experiments and wrote the paper. Alongside MR and SH performed data analysis. CD and SG were in charge of material preparation and involved in the data collection process. RM and CBA contributed to the writing of the paper and the conception of the study.

Funding No funding was received.

Declarations

Conflict of interest The author has no competing interests to declare that are relevant to the content of this article.

Ethical approval Not applicable.

References

1. B. Bensaude-Vincent, *Between Nature and Society: Biographies of Materials* (World Scientific, Singapore, 2022)
2. P.K. Mehta, *Concrete, structure, properties and materials* (Prentice-Hall, Englewood Cliffs, 1986), p. 450
3. Z.P. Bažant, Concrete fracture models: testing and practice. Eng. Fract. Mech. **69**, 165–205 (2001)
4. J. Ožbolt, J. Bošnjak, E. Sola, Dynamic fracture of concrete compact tension specimen: experimental and numerical study. Int. J. Solids Struct. **50**, 4270–4278 (2013)
5. J. Xiao, H. Schneider, C. Dönnecke, G. König, Wedge splitting test on fracture behaviour of ultra high strength concrete. Constr. Build. Mater. **18**, 359–365 (2004)
6. A. Hillerborg, The theoretical basis of a method to determine the fracture energy gf of concrete. Mater. Struct. **18**, 291–296 (1985)
7. V.D. Ho et al., Investigating the reinforcing mechanism and optimized dosage of pristine graphene for enhancing mechanical strengths of cementitious composites. RSC Adv. **10**, 42777–42789 (2020)
8. S. Yang, C. Zhang, Notch depth and root radius effects on quasi-brittle fracture of materials related to grain size. Ceram. Int. **48**, 23706–23712 (2022)
9. W. Meng, Y. Yao, B. Mobasher, K.H. Khayat, Effects of loading rate and notch-to-depth ratio of notched beams on flexural performance of ultra-high-performance concrete. Cem. Concr. Compos. **83**, 349–359 (2017)
10. M.P. Wagoner, W.G. Buttlar, G.H. Paulino, Development of a single-edge notched beam test for asphalt concrete mixtures. J. Test. Eval. **33**, 452–460 (2005)
11. X. Sun et al., Fracture performance and numerical simulation of basalt fiber concrete using three-point bending test on notched beam. Constr. Build. Mater. **225**, 788–800 (2019)
12. S. Ziegeldorf, H.S. Müller, H.K. Hilsdorf, A model law for the notch sensitivity of brittle materials. Cem. Concr. Res. **10**, 589–599 (1980)
13. H. Šimonová et al., Mechanical fracture parameters of cement based mortars with waste glass powder. Proc. Eng. **190**, 86–91 (2017)
14. A. Gharpure, J.W. Heim, R.L.V. Wal, Characterization and hazard identification of respirable cement and concrete dust from construction activities. Int. J. Environ. Res. Public Health **18**(19), 10126 (2021)
15. S. Ribeiro, J.A. Rodrigues, Influence of notch shape and preparation on the maximum load and fracture energy of mortars evaluated by the wedge splitting method for stable crack propagation. Ceramica **326**, 126733 (2009)
16. H. Yoshizawa, S. Wignarajah, H. Saito, Study on laser cutting of concrete. Trans. Jpn. Weld. Soc. **20**, 31–36 (1989)
17. S. Muto, K. Tei, T. Fujioka, Laser cutting for thick concrete by multi-pass technique. Chin. Opt. Lett. **5**, S39–S41 (2007)
18. T. Rümenapp, A. Lenk, Laser beam cutting of concrete. Key Eng. Mater. **250**, 257–261 (2003)
19. D. Lee, Y. Seo, S. Pyo, Effect of laser speed on cutting characteristics of cement-based materials. Materials **11**(7), 1055 (2018)
20. M. Moini, J. Olek, J.P. Youngblood, B. Magee, P.D. Zavattieri, Additive manufacturing and performance of architectured cement-based materials. Adv. Mater. **30**, 1802123 (2018)
21. R. Moini et al., Quantitative microstructural investigation of 3d-printed and cast cement pastes using micro-computed tomography and image analysis. Cem. Concr. Res. **147**, 106493 (2021)
22. J.J.-A. Wang, K.C. Liu, D. Naus, A new test method for determining the fracture toughness ofconcrete materials. Cem. Concr. Res. **40**(3), 497–499 (2010)
23. D. Lee, S. Pyo, Experimental investigation of multi-mode fiber laser cutting of cement mortar. Materials **11**, 278 (2018)
24. T. Kim, J. Olek, Effects of sample preparation and interpretation of thermogravimetric curves on calcium hydroxide in hydrated pastes and mortars. Transport. Rese. Rec. **2290**, 10–18 (2012)
25. G.A. Khoury, Effect of fire on concrete and concrete structures. Progress Struct. Eng. Mater. **2**, 429–447 (2000)
26. M. Lahoti, K.H. Tan, E.H. Yang, A critical review of geopolymer properties for structural fire-resistance applications. Constr. Build. Mater. **221**, 514–526 (2019)
27. D. Ravindra, M. Ghantasala, J. Patten, Effect of applied load, cutting speed and laser power on the material deformation and removal of semiconductors. Trans. 40th North Am. Manufact. Res. Inst. SME. 40, 544-550 (2012)
28. Savriama, G., Jarry, V., Barreau, L., Boulmer-Leborgne, C. & Semmar, N. A novel patterning effect during high frequency laser micro-cutting of hard ceramics for microelectronics applications. 302 (2014)